Kim Daehyun (Orcid ID: 0000-0001-9233-2747)

WISHE-moisture mode in an aquaplanet simulation

Xiaoming Shi[1], Daehyun Kim[2*], Ángel F. Adames[3], and Jai Sukhatme[4]

[1]Civil and Environmental Engineering, University of California, Berkeley, CA

[2]Department of Atmospheric Sciences, University of Washington, Seattle, WA

[3]Department of Climate and Space Science and Engineering, University of Michigan, Ann Arbor, MI

[4]Centre for Atmospheric and Oceanic Sciences, Indian Institute of Science, Bangalore, India

*Corresponding author: Daehyun Kim (daehyun@uw.edu)

†Address: Department of Atmospheric Sciences, University of Washington, Seattle, WA 98195-1640

Key Points:

- An aquaplanet simulation exhibits a mode of planetary-scale (wavenumber 1), eastward propagating intraseasonal variability.
- Moist static energy budget and mechanism denial experiments suggest that this mode is the linear WISHE-moisture mode of Fuchs and Raymond.
- The WISHE and longwave cloud-radiation feedbacks serve as scale-selection mechanisms for the intraseasonal variability.

This is the author manuscript accepted for publication and has undergone full peer review but has not been through the copyediting, typesetting, pagination and proofreading process, which may lead to differences between this version and the Version of Record. Please cite this article as doi: 10.1029/2018MS001441

Abstract

This study aims to understand the nature of the tropical intraseasonal oscillations (ISOs) in an aquaplanet simulation performed using GFDL's AM2.1 with a uniform sea surface temperature within the deep tropics. The simulated ISO resembles the observed Madden-Julian Oscillation in that the spectral peak in precipitation appears at zonal wavenumber 1 and a period of ~60 days. Vertically-integrated moist static energy budget of the simulated ISO shows that enhanced latent heat flux to the east of anomalously active convection causes eastward propagation of the ISO mode, which is weakly opposed by horizontal moisture advection. A series of mechanism-denial experiments are conducted either by homogenizing select variables – surface wind stress, longwave radiative heating, and surface evaporation – with their zonal means from the control simulation, or by suppressing free-tropospheric moisture variation. Results of the mechanism-denial experiments show that the simulated ISO disappears when the interactive surface evaporation is disabled, suggesting that the wind-induced surface heat exchange (WISHE) mechanism is essential to the simulated ISO. Longwave cloud-radiation feedbacks and moisture-convection feedbacks affect horizontal scale and phase speed of the simulated ISO, respectively. Our results strongly suggest that the simulated ISO is the linear WISHE-moisture mode of Fuchs and Raymond under horizontally uniform boundary conditions.

1 Introduction

Aquaplanet simulations – running numerical models of the atmosphere on a water-covered Earth – are in a unique position in the hierarchy of atmospheric modeling systems and have served an important role in understanding the dynamics of various atmospheric phenomena (Blackburn and Hoskins 2013). The tropical intraseasonal oscillation (ISO) is no exception in this regard. The first aquaplanet simulation using an atmospheric general circulation model (AGCM) was performed by Hayashi and Sumi (1986), who observed a 30-40-day tropical ISO in their simulation. Their results demonstrated that aquaplanet simulations are a useful method to study the tropical ISO. Since then, many modeling studies of the tropical ISO have employed the aquaplanet configuration (e.g. *Swinbank et al*. 1998; *Lee et al*. 2001; *Grabowski* 2003; *Kim et al.* 2008; *Andersen and Kuang* 2012; *Kang et al.* 2013; *Arnold et al*. 2013; *Hsu and Murakami* 2014; Leroux et al. 2016; Das et al. 2016). Readers are referred to Leroux et al. (2016) for a brief review of previous aquaplanet modeling studies on the tropical intraseasonal variability.

The Madden-Julian oscillation (MJO, *Madden and Julian* 1971, 1972) is the dominant mode of tropical intraseasonal variability whose influence on the global weather-climate system is well-documented (*Zhang* 2013). While the salient features of the MJO – planetary zonal scale, 30-60-day period, and eastward propagation at ~ 5 m s^{-1} over the Indo-Pacific warm pool – have been well-known for many decades, our understanding of the MJO is still unsatisfactory.

One of the distinguishing features of the MJO is the strong spatial and temporal coupling between tropospheric water vapor and latent heat release (Myers and Waliser, 2003; Yasunaga and Mapes 2012), which is central to multiple recent theories for the MJO (Majda and Stechmann 2009; Sobel and Maloney 2012; Sobel and Maloney 2013; Adames and Kim, 2016; Wang and Chen 2016, Fuchs and Raymond 2017, FR17 hereafter). In the so-called "moisture mode theories", the processes that determine the growth and propagation of the large-scale moisture envelope also explain those of the MJO. With the common core concept, the different linear theories of the moisture mode emphasize different processes for MJO propagation, maintenance, and scale-selection. The processes that are suggested as key destabilization and planetary-scale selection mechanism of the MJO include a negative gross moist stability (GMS) or the moisture mode instability (Raymond and Fuchs 2009), the cloud-radiative feedbacks (Adames and Kim, 2016), and wind-induced surface heat exchange (WISHE) (Emanuel, 1987; Neelin et al., 1987; Fuchs and Raymond, 2017). Similarly, for the processes that drive the propagation of the MJO, horizontal moisture advection (Adames and Kim, 2016), frictional moisture convergence (Wang and Chen 2016), and WISHE (Fuchs and Raymond, 2017) have been emphasized.

All these theories share the common feature that they are based on zonally-symmetric mean states. Horizontally homogenous mean states without zonal or meridional SST gradients are sometimes used (Fuchs and Raymond 2017). Simulations on a zonally-symmetric aquaplanet could provide a useful framework to test the importance of the key mechanisms suggested by

different theories to simulated intraseasonal variability since the modeled mean state resembles those assumed by linear theory.

Many previous aquaplanet modeling studies have aimed at providing useful insights into the dynamics of the MJO. Inspired by the moisture mode theory, moist static energy (MSE) budget of ISOs simulated in aquaplanet simulations are analyzed. *Maloney et al.* [2010] showed based on the MSE budget that WISHE and horizontal moisture advection were key to the destabilization and eastward propagation of an MJO-like mode in their simulation. *Andersen and Kuang* [2012] performed aquaplanet simulation with the Superparameterized Community Atmospheric Model (SPCAM) and suggested the longwave cloud-radiation feedbacks, which were the main source of MSE, played a key role in the growth of the MJO-like disturbance in their simulations. Simulations of a rotating radiative-convective equilibrium simulation by Arnold and Randall (2015) further supported the role of longwave radiative heating in the maintenance of the MJO. The aquaplanet modeling studies have often accompanied by mechanism-denial experiments [Lee et al. 2001; *Chao and Chen* 2001; Grabowski 2003; *Maloney and Sobel* 2004; *Sobel et al*. 2010; *Kim et al*. 2011]. For example, *Lee et al.* [2001] specified the zonal mean net radiative heating rate and found that longwave-cloud interaction had negative effects on the tropical intraseasonal variability by effectively exciting small-scale disturbances. *Grabowski* [2003] tested the role of wind-induced surface heat exchange (WISHE) and cloud-radiation interaction in the maintenance of an MJO-like disturbance and found that WISHE had a moderate importance in the development of the disturbance, while cloud-radiation interaction played a minor role.

The current study is motivated by the results of a global rotating radiative-convective equilibrium simulation performed by Shi and Bretherton (2014) using the Geophysical Fluid Dynamics Laboratory (GFDL)'s AM2.1 (*Anderson et al*., 2004). In their simulation, AM2.1 was driven by globally uniform sea surface temperature (SST) on an aquaplanet. Shi and Bretherton (2014) unexpectedly found an MJO-like intraseasonal variability in their simulation. It was unexpected because it has been documented that AM2.1 cannot realistically simulate the MJO with the observed SST and the full geography (*Kim et al. 2011*). The goal of the current work is to illuminate the dynamics of the simulated ISO mode by analyzing the moist static energy budget of the mode and also by performing a series of mechanism-denial simulations.

The structure of the current document is as follows. Section 2 describes the simulations performed, including the mechanism-denial experiments. In Section 3, we examine vertically-resolved moisture budget of the simulated ISO mode. Section 4 presents the results of the mechanism-denial simulations. A summary and discussions on the nature of the simulated ISO mode are given in Section 5.

2 Model and simulation design

2.1 *Numerical model*

The AGCM used in this study is the Geophysical Fluid Dynamics Laboratory (GFDL)'s AM2.1 (*Anderson et al*., 2004). Standard physics schemes and parameters of AM2.1 are adopted in our simulations. AM2.1 has a finite-volume dynamical core on a latitude-longitude grid (*Lin*, 2004), which in our simulations has a resolution of 1 latitude by 1.25 longitude, with 24 vertical levels. As detailed in Anderson et al. (2004), clouds and precipitation in AM2.1 are parameterized with the aid of prognostic variables for the cloud fraction and the specific humidities of cloud liquid water and cloud ice, and grid-scale fluxes of rain and snow are computed diagnostically from these prognostic fields (*Tiedtke* 1993; *Rotstayn*, 1997; *Rotstayn et al*., 2000). Cumulus convection is represented by the Relaxed Arakawa-Schubert formulation of *Moorthi and Suarez* (1992). Readers interested in details of AM2.1 physics schemes or dynamics are referred to *Anderson et al*. (2004), and references therein.

2.2 *Control simulation*

The SST for our control aquaplanet simulation is uniform in the deep tropics between 15°S and 15°N and shows a gradual transition to 2℃ between 15°S/N to the South/North Poles (Fig. 1). This prescribed SST is zonally invariant. Note that by using this SST distribution, we attempt to reproduce the simulation analyzed by *Shi and Bretherton* (2014), except that we impose a meridional SST gradient poleward of 15°S/N in order to make the simulation more relevant to the Earth's climate.

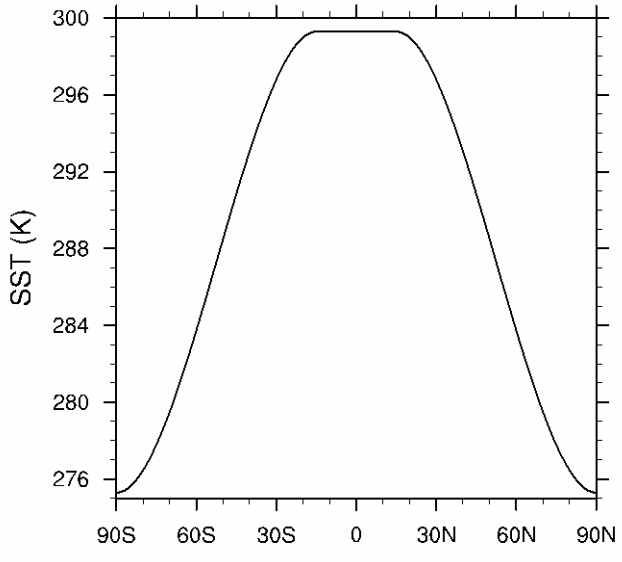

Figure 1. Prescribed sea surface temperature in the simulations

2.3 *Mechanism-denial experiments*

Based on the control simulation, we performed a series of mechanism-denial experiments, in which certain feedback processes are disabled by muting the variability of ~~some~~ key variables. Here in each experiment, the variability of a select field is eliminated or suppressed in the deep tropics between 15°S and 15°N. The target feedback process and experimental design of the mechanism-denial experiments are described below.

a) Nudge_q, Fixed_q

In the Nudge_q and Fixed_q simulations, perturbations in specific humidity q in the deep tropics above 850 hPa is *nudged* towards and *fixed* to the desired vertical profile, respectively. The reference profile is obtained from the control run. The Nudge_q experiment uses a 60-hour nudging time scale. By artificially suppressing and inhibiting free-tropospheric moisture variability, the Nudge_q and Fixed_q experiments test the role of moisture-wave coupling in the simulated ISO mode.

b) Fixed_tau

In the Fixed_tau experiment, the zonal mean surface wind stress from the control simulation is prescribed in the deep tropics. This disables the interaction of large-scale circulation with the friction-induced boundary layer convergence, which has been proposed a key process to MJO's eastward propagation (*Wang* 1988; *Wang and Rui* 1990; *Wang and Li* 1994; *Hsu and Li* 2012].

c) Fixed_Q_{LW}

As in the Fixed_tau experiment, the zonal mean longwave radiative heating rate is obtained from the control simulation and prescribed in the Fixed_Q_{LW} experiment. Therefore, the longwave cloud-radiation feedbacks are turned off in this simulation. The interaction of longwave cooling with MJO-induced moisture and cloud anomalies have been suggested as the dominant maintenance mechanism of the MJO (*Bony and Emanuel* 2005; *Andersen and Kuang* 2012; *Crueger and Stevens* 2015; Arnold and Randall 2015; *Adames and Kim* 2016).

d) Fixed_LH

In the Fixed_LH experiment, the interaction between large-scale circulation and surface latent heat flux is disabled by prescribing surface latent heat flux, which is obtained from the control simulation as the zonal mean value. This experiment tests the influence of wind-evaporation feedback or wind-induced surface heat exchange (WISHE) mechanism (*Emanuel* 1987*; Neelin et al.* 1987; *Yano and Emanuel* 1991; *Emanuel* 1993; Fuchs and Raymond 2017) on the MJO-like ISO mode.

Each experiment is run for 12 years. The first 2-year data are discarded as spin-up, and the last 10-year data are retained for analysis. Model data are archived with daily intervals for the analysis.

2.4 Regression maps

In each simulation, we define intraseasonal variability (ISV) index as the 20-100 day band-pass filtered precipitation in a $10^\circ \times 10^\circ$ square region centered at the Equator. The time series of ISV index is used to produce regression maps of other variables. We did not choose time/wavenumber-filtered anomalies to create the ISV index because the wavenumber, frequency, and propagation direction of the dominant mode change significantly from one experiment to another.

Following *Adames and Wallace* (2014), the regression map for each variable is obtained through the equation

$$\mathbf{D} = \mathbf{S}\,\mathbf{P}^{\mathrm{T}}/N \tag{1}$$

where $\mathbf{D}$ is the regression pattern, in dimensional units, for a two-dimensional matrix $\mathbf{S}$ that represents a variable field S, $\mathbf{P}$ is a standardized time series of the ISV index, and N is the sample size in days. The regression maps correspond to one-standard-deviation anomalies.

3 MJO-like ISO mode in the control simulation

In this section, we examine the mean state and the intraseasonal variability in the control simulation. Figure 2 shows the distribution of mean precipitation and precipitable water in the control simulation. The mean precipitation exhibits two ITCZs at around 15^o N/S, respectively. Except near the latitude of the ITCZs, mean moisture in the deep tropics exhibits very weak gradient in the meridional direction. The very weak horizontal moisture gradient suggests that the advection of mean moisture by perturbation winds would be small.

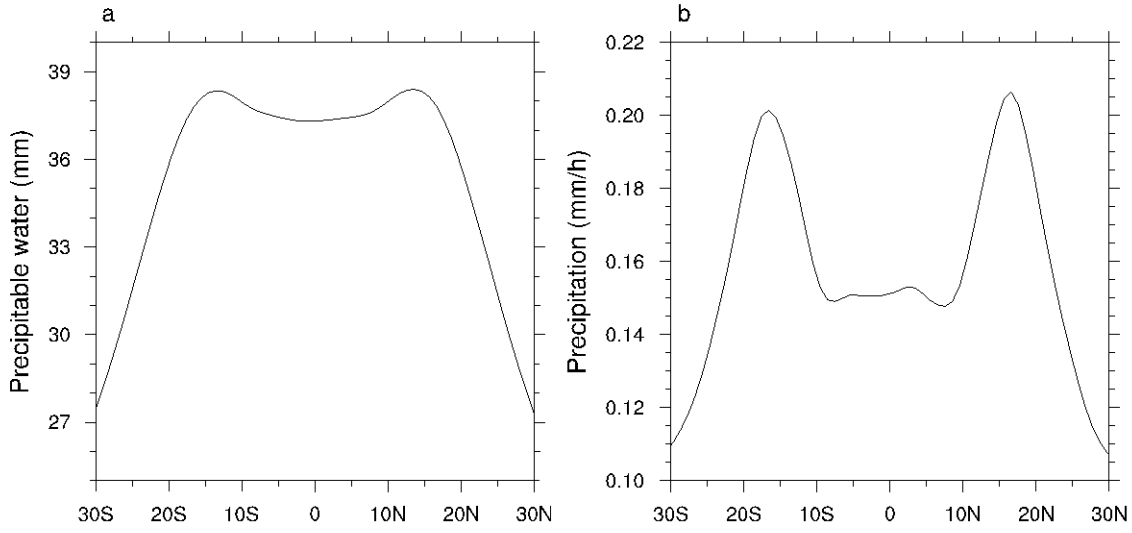

Figure 2. Time mean, zonal mean distribution of a) precipitable water (PW, mm) and b) precipitation rate (mm h^{-1}) in the control simulation.

Figure 3 shows the space-time spectrum of equatorial precipitation in the control simulation. Only the spectrum of the symmetric component is shown as it dominates the anti-symmetric component. Tropical variability in the control run is dominated by a wavenumber-1 mode that propagates eastward and has a period of about 60 days, resembling that of the observed MJO. Hereafter, we will call this MJO-like mode the aquaplanet ISO mode, or simply the ISO mode. It is also worthwhile to mention that due to strong surface easterlies (not shown), the power spectrum features a pronounced westward propagating signal.

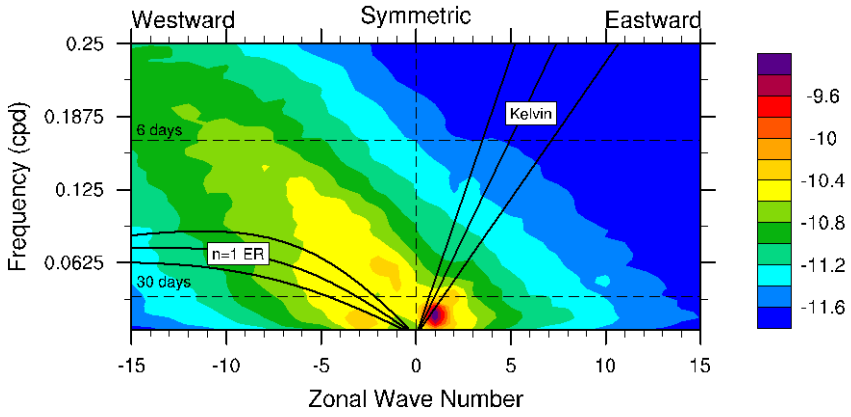

Figure 3 Space-time spectrum of the symmetric component of precipitation within between 15°S and 15°N in the control simulation.

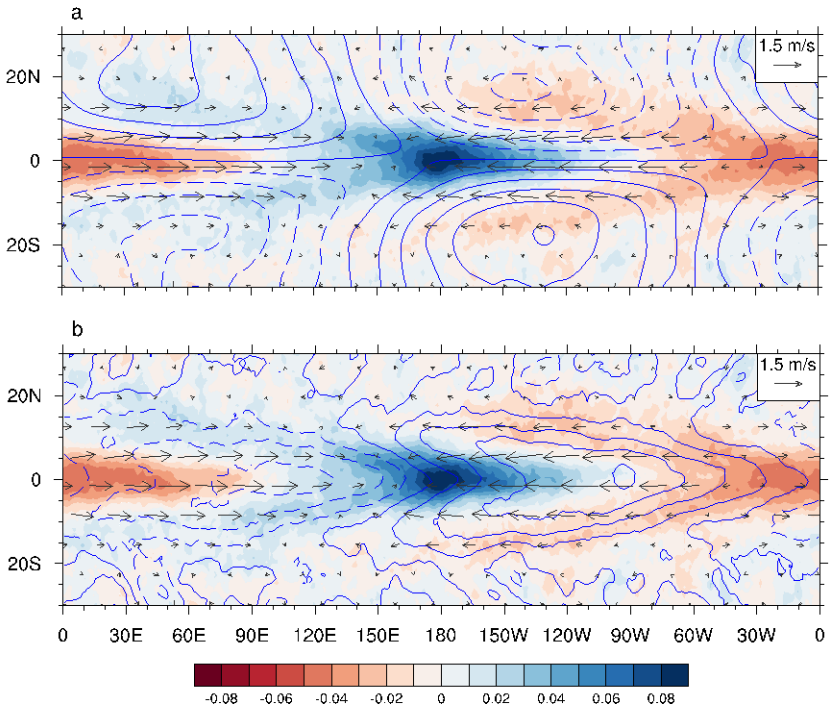

Figure 4. The regression map of precipitation (color), 850 hPa wind (vectors), 850 hPa streamfunction (contours in **a**) and surface evaporation (contours in **b**) onto the ISV index time series in the control simulations. Dashed contours indicate negative values. Units for precipitation is mm/h. Contour interval for evaporation is 0.004 mm/h.

The horizontal structure of the ISO mode in the control simulation is presented in Fig. 4, which shows regression maps of precipitation, 850hPa wind, 850hPa streamfunction and evaporation. All fields are dominated by wavenumber-1 structures. Near the equator, the low-tropospheric wind anomalies exhibit strong convergence at the location of maximum precipitation anomaly. This low-level convergence is much stronger in the zonal direction than in the meridional direction. The meridional wind anomalies are overall much weaker than the zonal wind anomalies. Away from the equator, streamfunction anomalies indicate a poleward flow at the longitude of and to the west of enhanced convection. This differs from the structure of the MJO in the reanalysis products, which has a poleward anomalous flow to the east of enhanced convection (e.g. *Kim et al.*, 2014, Adames and Wallace 2015). Fig. 4b shows evaporation anomalies in contours and the closed contour at 90°W and on the equator indicates the maximum. It shows that surface evaporation anomalies lead precipitation anomalies by about 90° in longitude, suggesting that enhanced surface latent heat flux to the east of enhanced convection may be responsible for the eastward propagation of the ISO mode. This phase relationship between precipitation and surface evaporation in the aquaplanet-simulated ISO mode contrasts with that of the observed MJO, in which evaporation is enhanced to the west of convection, not to the east (*Shinoda et al.*, 1998). Interestingly, both precipitation and surface evaporation show "swallowtails" to the west of maximum anomalies.

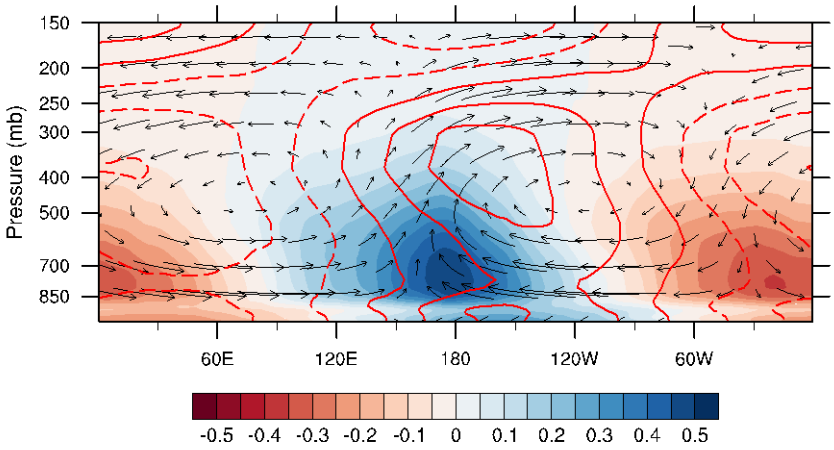

Figure 5. Regression map of mass flux (ρu and ρw), specific humidity (q; color shading) and temperature (T; contours) within 5°S and 5°N onto the time series of ISV index in the control simulation. The unit of $q$is g/kg. Contour interval for T is 0.1 K. $\rho w$is multiplied by a factor of 250 for better visualization.

Figure 5 shows the vertical structure of the aquaplanet ISO mode. The maximum positive moisture anomalies appear at the location of the maximum precipitation anomalies, suggesting a strong moisture-convection coupling in the ISO mode. Moisture anomalies tilt slightly westward with height. Due to the rearward tilting, moisture anomalies in the upper troposphere slightly lag precipitation anomalies. The mass flux anomalies show a strong low-level convergence and strong upper-level divergence slightly to the west of enhanced convection. Positive temperature anomalies are located to the east of positive moisture anomalies and tilt westward with height, showing that temperature anomalies are partly in phase with convection. This partly in-phase relation between temperature field and convection (diabatic heating) has been suggested as the destabilization mechanism of the WISHE-driven mode (*Emanuel et al*, 1994).

In order to understand the time evolution of the moisture anomalies, which are tightly coupled to convection, the column-integrated moist static energy (MSE) budget of the ISO mode is examined. The tendency of anomalous MSE is determined as follows,

$$\frac{\partial \langle h \rangle'}{\partial t} = -\langle V \cdot \nabla h \rangle' - \langle \omega \frac{\partial h}{\partial p} \rangle' + LH' + SH' + LW' + SW', \quad (2)$$

where h is MSE, LH and SH represent surface latent and sensible heat flux, respectively, and LW and SW represent column-integrated longwave and shortwave radiative heating, respectively. The primes in Eq. (2) correspond to 20-100 day filtered fields and the angled brackets represent column integration. The tendency and advection terms are obtained using the centered differencing scheme. Note that the MSE budget is not closed and a small residual term (about 10% of the amplitude of MSE tendency term) exists, due to the errors caused by the temporal interpolation of model output and by the use of the centered differencing scheme, which is not the same as the actual advection scheme of the model.

Figure 6 shows regression maps of each term in the MSE budget equation. Note that surface sensible heat flux and shortwave radiative heating terms are not shown as their magnitude is much smaller than those of the other terms in Eq. (2). The MSE tendency (contours) features increasing MSE anomalies, which is mostly due to moistening (not shown), to the east of enhanced convection and decreasing to the west. While the magnitude is relatively small, horizontal advection shows a positive (negative) tendency to the west (east) of enhanced convection, suggesting that horizontal moisture advection slows the eastward propagation of the

ISO mode. The drying tendency to the east of enhanced convection is possibly caused by the advection of dry air from the region with suppressed convection to the moist region with enhanced convection (Fig. 5). The overall weak intensity of horizontal advection likely results from the lack of zonal and meridional gradients in the climatology (Fig. 1).

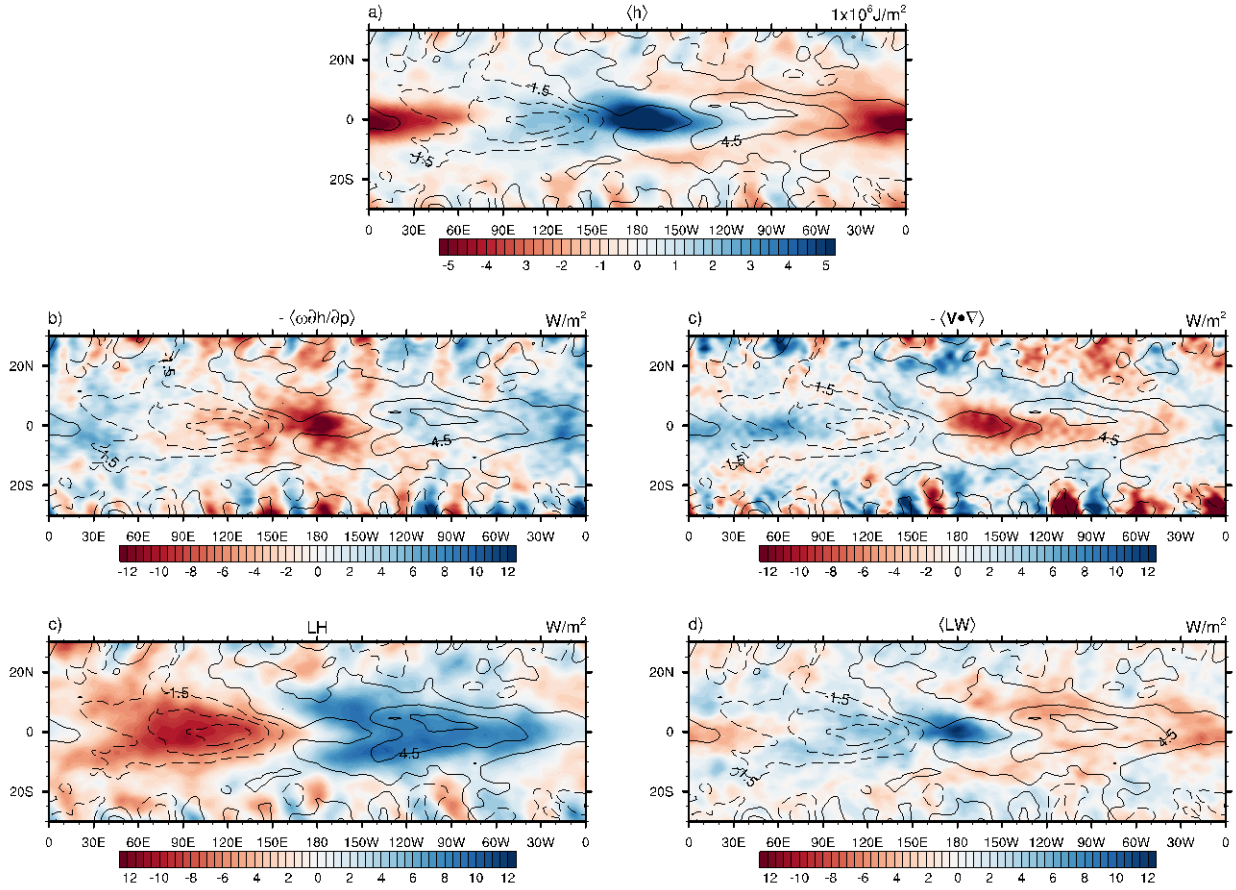

Figure 6: MSE tendency (contours) and various MSE budget terms (shaded) regressed onto the ISV index in the control simulation. a) MSE anomalies, b) horizontal advection, c) vertical advection, d) surface latent heat flux, and e) column-integrated longwave radiative heating.

Vertical advection of MSE provides a strong moistening tendency in the columns with enhanced convection and in the region surrounding it. This moistening is associated with the vertical gradient of moisture and strong upward motion in convection. Away from the center of enhanced convection, vertical advection associated with downward motion creates a strong drying tendency. Condensation exhibits the opposite phase to that of vertical advection. It

produces a drying tendency in the place with strong updrafts due to condensation, a moistening tendency in the place with subsidence due to suppressed condensation.

Figure 6d shows that shows that the moistening to the east of and drying to the west of the enhanced convection is dominated by surface evaporation. In fact, horizontal distribution of the anomalous surface latent heat flux is almost identical to that of the total tendency. And the magnitude of surface latent heat flux in the areas of large tendencies is much larger than that of the other terms. This result strongly suggest that the eastward propagation of the ISO mode is driven by the surface latent heat flux anomalies.

4 Mechanism-denial experiments

In this section, we examine results from the mechanism-denial experiments (Section 2.3) in order to seek a deeper understanding of the dynamics of the simulated ISO mode in our control simulation. Figure 7 shows the climatological mean distribution of precipitable water and precipitation in all simulations. Except for the Fixed_tau simulation, which exhibits slightly more precipitable water than other simulations, all simulations have a similar amount of precipitable water in the tropics with a weak meridional gradient of precipitable water in the deep tropics.

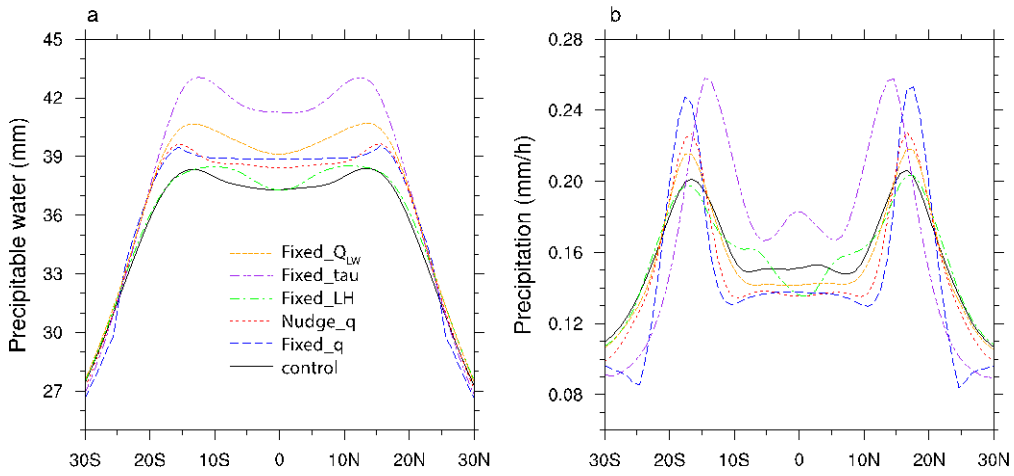

Figure 7: Time mean, zonal mean a) precipitable water and b) precipitation rate in all simulations.

Figure 8 shows the space-time spectra of equatorial precipitation in the mechanism denial experiments. The spectrum of the control simulation is shown again as a reference. The spectrum of Fixed_tau resembles that of the control simulation; intraseasonal variability in the Fixed_tau

experiment remains dominated by an eastward-propagating, wavenumber-1 mode with a period of about 60 days. This suggests that the interaction between lower-tropospheric circulation and surface wind stress is not the key mechanism governing the simulated ISO in the control simulation.

The Fixed_Q_{LW} simulation exhibits a significant change in the spectrum. Its intraseasonal variability is still dominated by eastward propagating waves, but the variability is spread over a wide wavenumber band from wavenumber 1 to 6, unlike in the control simulation, in which spectral power is concentrated on the wavenumber 1. Interestingly, the spectrum shows a dip at wavenumbers 2 and 3. This suggests that the longwave cloud-radiation feedback plays an important role in the scale-selection of intraseasonal variability, consistent with the theoretical arguments by *Adames and Kim* (2016). The spectral peak over the band of the convectively-coupled Kelvin waves becomes more prominent when compared to the control simulation. Kim et al. (2011) also found that turning off the longwave cloud-radiation feedback strengthens the convectively-coupled Kelvin wave at the expense of MJO variability.

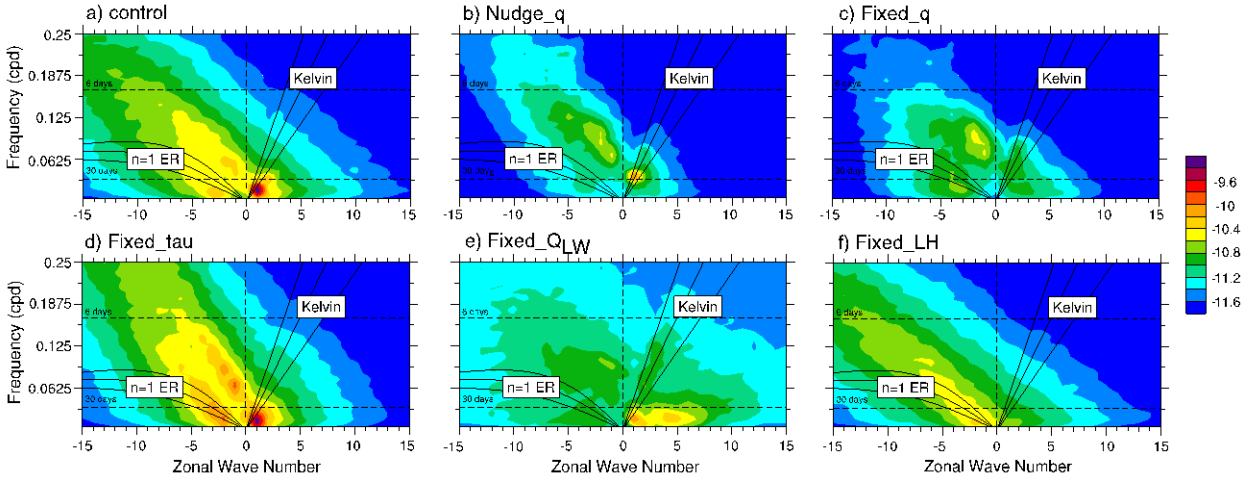

Figure 8: Space-time spectra of the symmetric component of precipitation within 15°S and 15°N in the simulations.

To test if the longwave cloud-radiation feedbacks in the control simulation are indeed scale-selective, we estimate the wavenumber dependence of the radiative feedback parameter *r*, which is defined by the following relationship,

$$R' = rP', \qquad (3)$$

where $R'$and $P'$are anomalies of outgoing longwave radiation at the top of the atmosphere and precipitation at the surface, respectively. Following *Adames and Kim* (2016), we decompose the 20-100-day filtered $R'$and P'within 15°S and 15°N into contributions from individual zonal wavenumbers, and compute *r* for each wavenumber through linear least squares regression. Data on each latitude circle are computed, and the averaged feedback parameter as a function of zonal wavenumber is shown in Fig. 9, which suggests that *r* decreases with wavenumber in general and the cloud-radiation feedback is indeed scale-selective. The relation between *r* and zonal wavenumber *k* can be depicted by the following empirical formula,

$$r = r_0 e^{-L_r k}. \qquad (4)$$

Least squares fitting with data in Fig. 9 results in $r_0 = 0.22$, and $L_r = 244$km, consistent with the estimates of *Adames and Kim* (2016) using observational data.

However, an intriguing detail of Fig. 9 is that the radiative feedback is not strongest at wavenumber 1, instead, the feedback parameter peaks at wavenumbers 2 and 3, while the estimation based on observational data suggests *r* is largest at wavenumber 1 (*Adames and Kim 2016*). This disparity may be caused by inaccurate parameterization of convection and clouds in the model or from uncertainty in the calculation of *r* for each zonal wavenumber. That the cloud-radiation feedbacks are strongest at wavenumbers 2 and 3, not at wavenumber 1, may also suggest that while cloud-radiation feedback is important for scale selection in the control simulation, some other mechanism, such as the WISHE feedback (*Fuchs and Raymond* 2017), coexists to selectively amplify the intraseasonal variance at wavenumber 1 in the model. Indeed, while the low-frequency variance spreads between wavenumber 1 to 6 in Fig. 8e, wavenumber 1 still exhibits slightly larger variance than wavenumbers 2 and 3, supporting this hypothesis.

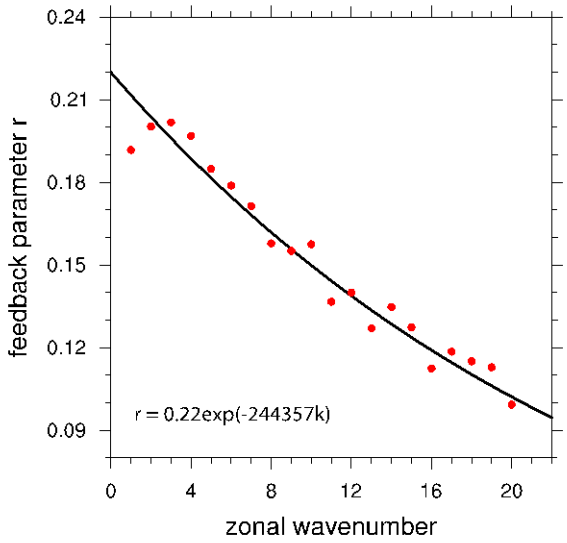

Figure 9: Cloud-radiation feedback parameter *r* as a function of zonal wavenumber (red dots). The black solid curve is the linear least squares regression.

In the Nudge_q experiment, in which the free-tropospheric moisture variability is constrained, the wavenumber-1 mode shows a notable increase in frequency, and a significant drop in variability (Fig. 8b). Further increase in frequency and decrease in power are observed when free-tropospheric moisture is not allowed to vary at all in the Fixed_q experiment (Fig. 8c). The increase in the phase speed of the dominant ISO mode can also be seen in the space-time power spectrum 850-hPa zonal wind (Figure 10). These findings suggest that the wave-moisture coupling modulates the propagation speed and amplitude of the ISO mode in the control simulation. Note that

In the Fixed_LH experiment, the MJO-like ISO mode disappears (Fig. 8f). The intraseasonal variability is dominated by westward-propagating components. That disabling WISHE feedback completely shuts off the MJO-like ISO mode with only minimal changes in the background state (Fig. 7) strongly suggest that the WISHE feedback is the key mechanism for the maintenance of the MJO-like ISO mode. This may also suggest that the WISHE feedback prefers the wavenumber-1 mode, which is consistent with that the wavenumber-1 mode still exists in the Fixed_Q_{LW} simulation. Although, the existence of wavenumber-1 mode in the Fixed_Q_{LW} simulation may also benefit from the absence of zonal SST gradient, which, according to *Maloney et al.* (2010), could shift the dominant wavenumber towards lower ones.

In Figure 10, the horizontal structures of the ISO modes in the mechanism-denial experiments are shown. Note that results from Fixed_LH and Fixed_q are not shown because their regression maps do not show any significant feature due to the lack of dominant wave signal. The Fixed_tau experiment shows a clear wavenumber-1 structure in circulation, evaporation and precipitation field. Evaporation leads precipitation by about 90° in longitude. The convergence of low-level wind appears to be purely zonal, and no significant meridional component is shown in the wind field. In contrast, the Fixed_Q_{LW} experiment shows a much smaller scale in the regressed response of precipitation and evaporation. Wind field retains the wavenumber-1 structure, but the response is much weaker than that in other experiments. Note that Arnold and Randall (2015) also found in their aquaplanet simulations that removing longwave cloud-radiation feedbacks weakens the MJO-like variability. The Nudge_q simulation, on the other hand, exhibits wavenumber-1 structure in all three fields, albeit the responses are weaker compared with the control simulation (Fig. 4b).

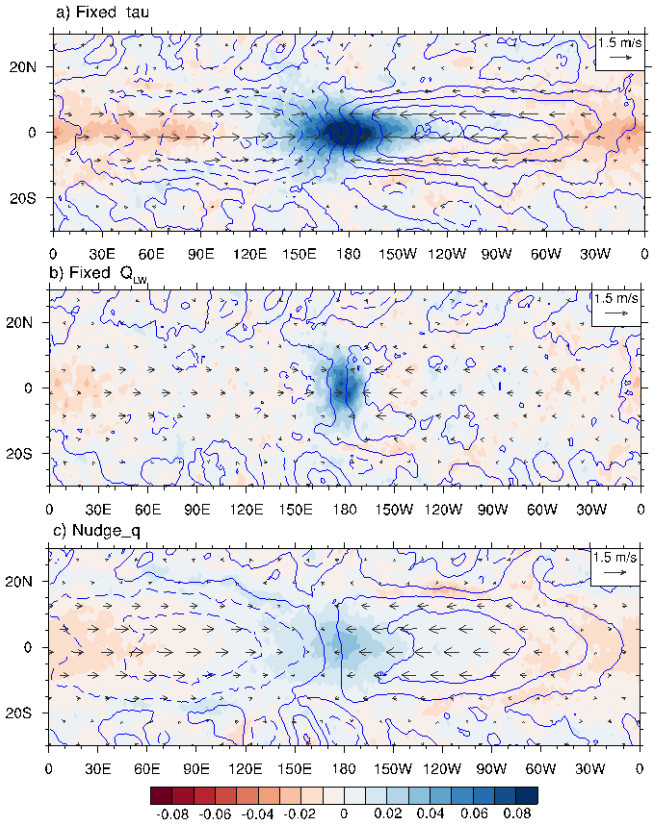

Figure 10 The regression map of precipitation (color), 850 hPa wind (vectors), and surface evaporation (contours) onto the ISV index time series in the noS, noL, and nuQ simulations. Dashed contours indicate negative values.

Figure 11 shows vertical structures of the dominant ISO modes in the mechanism denial experiments. Again, the Fixed_tau experiment exhibits well-defined wavenumber-1 structure. Low-level winds converge at the location of enhanced convection, producing strong upward motion and a positive anomaly of specific humidity, and upper winds diverge above the enhanced convection. Strong subsidence exists at the longitudes about 180^{o} away from the enhanced convection, producing a dry anomaly in the corresponding location. Upward motion in the control simulation exhibits a slight eastward tilting with height in the column with enhanced convection, but upward motions in the Fixed_tau run is upright in the center of convection.

The Fixed_Q_{LW} simulation, in contrast, exhibits weaker, more localized response in all fields. The upward motion in Fixed_Q_{LW} tilts westward with height. The moisture anomaly near the center of enhanced convection appears as a narrow plume, and a weak dry anomaly exists to the immediate east of the moist anomaly. The wind field in Fixed_Q_{LW} seems to have wavenumber-1 structure, but the downward motion to the immediate east of upward motion anomalies is stronger than the downward motion response 180^{o} away. These features all suggest eliminating radiation feedback leads to a shrinking in the spatial scale of the ISO mode.

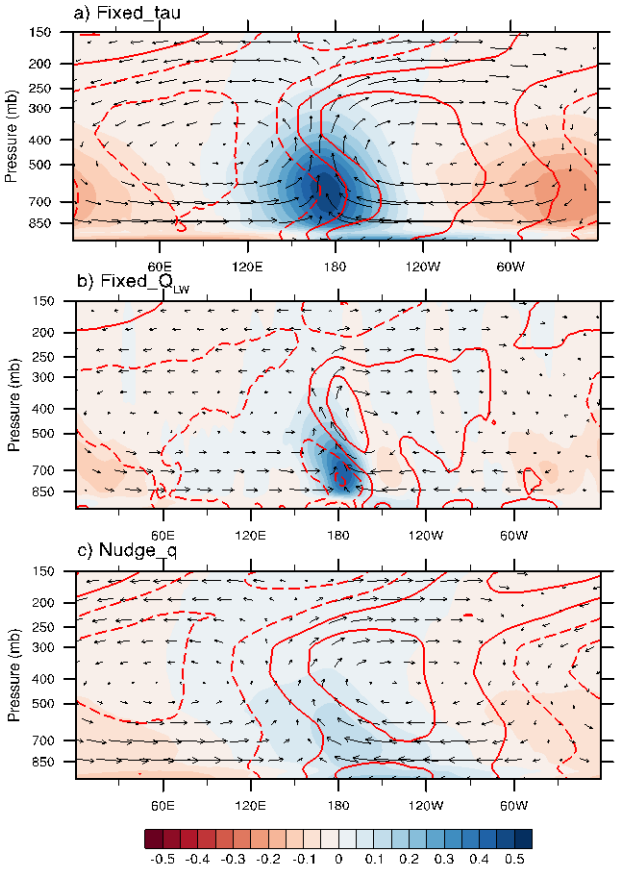

Figure 11: Regression map of mass flux (ρu and ρw), specific humidity (q; color shading) and temperature (T; contours) within 5°S and 5°N onto the time series of ISV index. The unit of q is g/kg. Contour interval for T is 0.1 K. ρw is multiplied by a factor of 250 for better visualization.

As expected, moisture anomalies are much weaker in the Nudge_q experiment than in the control simulation. But the moisture field exhibits well-defined wavenumber-1 structure, with moist anomaly being in the column with enhanced convection and dry anomaly 180° away. Moisture anomalies tilt westward with height. Temperature anomalies exhibit a pattern similar to that in the control simulation. Wind field in the Nudge_q experiment resembles that of the control simulation, with a clear wavenumber-1 structure.

5 Discussion

We find that the salient features of the aquaplanet ISO mode in the control simulation resemble that of the WISHE-moisture mode of FR17. FR17 assumed a basic state that has no horizontal moisture gradient. This is similar to our configuration with a flat SST in the deep tropics. This makes horizontal advection of moisture play a negligible role in our aquaplanet ISO mode and in the WISHE-moisture mode of FR17. When a realistic moisture gradient is considered, horizontal advection becomes a dominating mechanism for eastward propagation in a similar moisture mode model of Adames and Kim (2016).

Phase speed of the WISHE-moisture mode of FR17 increases with the moisture relaxation rate (their α parameter), which is equivalent to an inverse of the moisture relaxation time scale. In this sense, waves in our Nudge_q and Fixed_q would experience a shorter relaxation time scale, hence a greater moisture relaxation rate. Indeed, the moisture relaxation time scale, computed with 20-100-day band-passed tropical precipitation and precipitable water, in our control, Nudge_q, and Fixed_q simulations are 32.6, 24.6, and 10.4 hours, respectively. Therefore, the increases in the phase speed of the aquaplanet ISO mode in the Nudged_q and Fixed_q experiments are consistent with what FR17's dispersion relationship of the WISHE-moisture mode predicts.

In the WISHE-moisture mode of FR17, the WISHE mechanism is the only necessary process for instability while the cloud-radiation interaction could also provide an additional amplifying mechanism. In our mechanism-denial simulations, the aquaplanet-simulated ISO mode disappears only when the WISHE mechanism is turned off (Fixed_LH). When the longwave cloud-radiation interaction is disabled, the variance of the ISO mode was weakened, and intraseasonal variability still maximizes at wavenumber 1 (Fixed_Q_{LW}), again being consistent with the WISHE-moisture mode of FR17. Unlike the WISHE-moisture mode of FR17, in which the scale-selection of a wavenumber-1 mode is more pronounced without the cloud-radiation interaction (FR17's Figure 2), however, the results of the Fixed_Q_{LW} experiment suggest that the cloud-radiation feedbacks also play an important role in the scale selection of the aquaplanet ISO mode.

The results from the Nudge_q and Fixed_q experiments can also be shown to be consistent with the FR17 framework. We will modify their moisture equation (Eq. 11 in FR17) to include the nudging term used in our experiments:

$$\frac{\partial q'}{\partial t} = w'\Gamma_q - s_q - \frac{q'}{\tau_n}. \qquad (5)$$

The RHS terms are vertical moisture advection with Γ_q being the vertical moisture gradient, the moisture sources and sinks s_q, and the moisture nudging term where τ_n is a nudging timescale. In this simplified framework, adding the nudging term can be considered as increasing the GMS Γ. We can define a new GMS Γ^*that incorporates the effects of moisture nudging, which is expressed as follows

$$\Gamma^* = \Gamma + \frac{1}{\widetilde{\alpha}\tau_n}. \qquad (6)$$

Where $\widetilde{\alpha}$ is a moisture relaxation timescale, which is inversely proportional to the convective moisture adjustment timescale τ_c (Adames and Kim 2016, Jiang et al. 2016). The dispersion relation for the v=0 case discussed in FR17 with the new GMS is as follows (their Eq. 25)

$$\Omega^3 + i\alpha\Omega^2 - \kappa^2\Omega = -\alpha\kappa(\Lambda + i\Gamma^*\kappa). \qquad (7)$$

Where Ω is a nondimensional frequency, α is a nondimensional convective relaxation frequency, and κ is a nondimensional zonal wavenumber. The dispersion relation for values of $\Gamma^*$of 0, 0.1 and 0.2 are shown in Fig 14. Consistent with the results from the Nudge_q and Fixed_q experiments (Fig. 8), we see that the moist wave accelerates and exhibits weaker growth. Thus, the FR17 model can explain not only the results of the Fixed_LH experiment but also explains results of the Nudge_q and Fixed_q experiments.

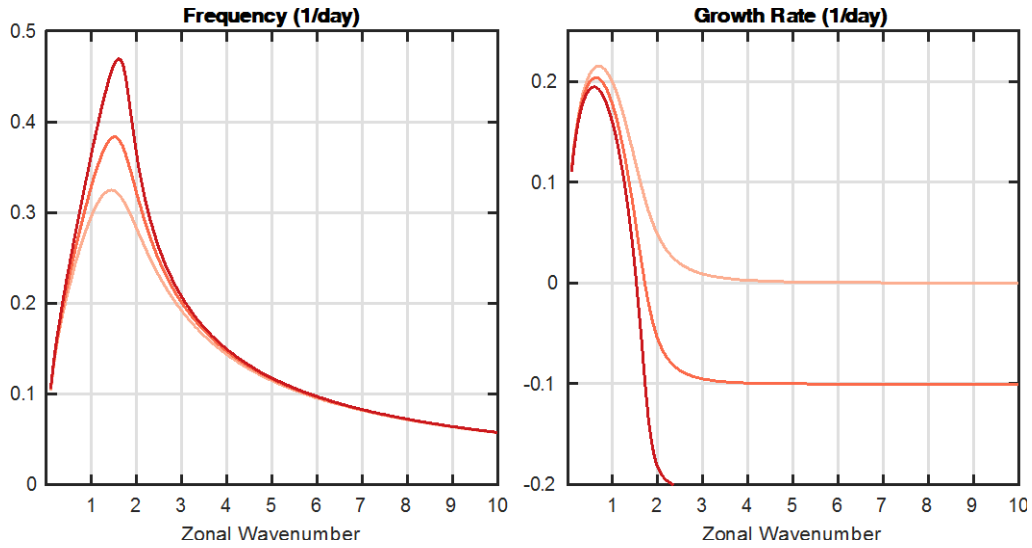

Figure 12: Frequency (left) and growth rate (right) of the growing mode obtained from the dispersion relation in Eq. 7. The lines correspond to the solutions for Γ^* values of 0, 0.1 and 0.2, respectively. Darker red shading indicates a larger value of Γ^*. All other values used here are as in FR17

6 Summary and Conclusions

In this study, we attempted to understand the nature of intraseasonal variability in an aquaplanet simulation whose spectral character resembles that of the observed MJO. The aquaplanet simulation was performed using GFDL's atmosphere model AM2.1 with a flat SST distribution in the deep tropics. The MJO-like ISO mode appeared in the aquaplanet simulation propagates eastward with a period of about 60 days and is spatially dominated by wavenumber-1 structures. In order to gain insight into the propagation mechanism of the ISO mode, we examined a vertically-resolved moisture budget of the ISO mode. We also performed a series of mechanism-denial experiments to shed light on the macroscopic feedback processes controlling the wave characteristics of the ISO mode.

The column-integrated MSE budget of the aquaplanet-simulated ISO mode suggested that enhanced surface evaporation to the east of anomalous convection leads the eastward propagation of the ISO mode. Horizontal advection of MSE causes a weak drying tendency to the east of enhanced convection. It is worthwhile to mention that despite their similar wave characteristics, the aquaplanet-simulated ISO mode and the observed MJO show a stark contrast in their moisture budget. Most notably, horizontal advection of MSE causes a weak drying tendency to the east of enhanced convection in the aquaplanet ISO mode, a feature that is distinct

from that of the observed MJO, in which horizontal MSE advection plays the dominant role in the propagation of the MJO. Also, enhanced surface evaporation is centered to the east of enhanced convection in the MJO-like ISO mode, while the opposite phase relation is true in the observed MJO. This difference could be a reflection of the mean state differences in the model and observations, or differences in the dynamics. Either difference could potentially explain why AM2.1 does not produce MJO-like variability with a realistic configuration, but produces a strong ISO in the simplified configuration analyzed here.

In the mechanism-denial experiments, the interactions of waves with i) free-tropospheric moisture, ii) surface wind stress, iii) long-wave radiative heating, and iv) surface latent heat flux are suppressed or inhibited to illuminate the roles that individual processes play in determining the characteristics of the ISO mode. The results of the mechanism-denial experiments are summarized in the following.

- The wave-moisture coupling affects the phase speed of the ISO mode, which increases progressively as the moisture is decoupled from the wave (Nudged_q and Fixed_q).
- The role of surface wind stress is *insignificant*. An MJO-like ISO mode appears even without interactive surface wind stress (Fixed_tau) and its wave characteristics are almost identical to that in the control simulation. This result suggests that frictional moisture convergence is not central to the simulated ISO.
- The longwave radiative feedbacks are essential in the scale-selection of the MJO-like ISO mode. When the longwave cloud-radiation feedbacks are disabled (Fixed_Q_{LW}), the intraseasonal variability of precipitation is spread between wavenumber 1 to 6, instead of concentrating on wavenumber-1. The longwave cloud-radiative feedbacks strength is scale-selective in general, as suggested by observations (*Adames and Kim* 2016). However, the radiative feedback parameter peaks at zonal wavenumbers 2 and 3 in lieu of 1, implying that cloud-radiation feedbacks are not the only mechanism responsible for the scale-selection of the ISO mode.
- The surface latent heat flux feedbacks are found to be critical to the aqua-planet simulated ISO mode, which disappears when surface evaporation is non-interactive (Fixed_LH).

The results of our MSE budget analysis and mechanism-denial experiments collectively suggest that the ISO mode in the control simulation is a mode whose existence relies on the surface latent heat flux feedbacks, whose scale is set by the surface latent heat flux and cloud-radiation feedbacks, and whose propagation speed is determined by its coupling with moisture and hence convection. These salient features of the aquaplanet ISO mode resemble that of the WISHE-moisture mode of *Fuchs and Raymond* (2017). Based on our results, it was hypothesized that the aquaplanet-simulated ISO mode in the control simulation is a manifestation of the WISHE-moisture mode of Fuchs and Raymond (2017).

It is worthwhile to note that the effects of specific feedback processes (e.g., cloud-radiation feedbacks and WISHE) on the simulated ISO mode in a model would be strongly dependent on the way the model represents relevant sub-grid scale processes. For example, the longwave cloud-radiation feedbacks would be stronger if the model convection scheme detrains more water vapor and cloud hydrometeors in the upper levels, if the upper clouds are optically thicker and last longer. Likewise, strength of WISHE would be affected by the boundary layer and surface flux schemes. Performing the mechanism-denial simulations using multiple models would help reduce the uncertainty associated with those in the parameterization schemes.

Aquaplanet simulations have become a popular framework in which one can study atmospheric phenomena in a simpler environment (Blackburn and Hoskins 2013). The current study presented another example of how such a framework can be useful in understanding tropical intraseasonal variability. Our results strongly suggest that the WISHE-moisture mode of FR17 exists, while leaving another important question unanswered: is the aquaplanet-simulated ISO mode is a manifestation of the observed MJO, or a different mode? If the observed MJO is indeed a WISHE moisture mode, it probably means that the WISHE feedback is central to the observed MJO, with the cloud-radiation feedback playing a secondary role in the scale-selection mechanism. In this case, it is possible that the WISHE feedback is somehow too weak or some other misrepresented circulation details suppress it significantly when AM2.1 is run with realistic configuration, and therefore the model no longer exhibits the MJO. Another possibility is that the WISHE feedback is not the dominant mechanism for the observed MJO, which implies that the aquaplanet-simulated ISO mode is not exactly a manifestation of the observed MJO. If the eastward propagation of the observed MJO is dominated by some other mechanisms, such as horizontal advection processes which are extremely weak in our aquaplanet simulations, it is impossible to simulate the MJO with our experimental design (flat tropical SST). The lack of the MJO in the simulation with realistic topography and SST can then probably be explained by biases in the horizontal moisture gradient. It is worth noting that a study by *Leroux et al* (2016) found that some models are able to simulate ISO when they have a warm pool and not with zonally symmetric SST conditions, suggesting that the horizontal distribution of the boundary condition can influence whether or not a model can represent an MJO-like ISO mode. Further modeling and theoretical studies are warranted to address this important question.

Acknowledgments

XS was supported by National Science Foundation (NSF) Grants AGS-1503860. DK was supported by National Aeronautics and Space Administration Grant 80NSSC17K0227, by the Korea Meteorological Administration Research and Development Program under grant KMI2018-03110. This work was facilitated through the use of advanced computational, storage, and networking infrastructure provided by the Hyak supercomputer system at the University of Washington. We thank Mike Wallace, Kerry Emanuel, and Željka Fuchs for their constructive comments that helped improve the manuscript. All data used in this manuscript are provided at https://github.com/shixm-cloud/WISHE2018.

References

Adames, Á. F., and J. M. Wallace (2014): Three-dimensional structure and evolution of the MJO and its relation to the mean flow. *J. Atmos. Sci.*, 71, 2007–2026, doi:10.1175/JAS-D-13-0254.1.

Adames, Á. F., and J. M. Wallace (2015): Three-dimensional structure and evolution of the moisture field in the MJO. *J. Atmos. Sci.*, **72**, 3733–3754, doi:10.1175/JAS-D-15-0003.1.

Adames, Á.F. and D. Kim (2016): The MJO as a Dispersive, Convectively Coupled Moisture Wave: Theory and Observations. *J. Atmos. Sci.*, **73**, 913–941, doi: 10.1175/JAS-D-15-0170.1.

Adames, Á.F., J.M. Wallace, and J.M. Monteiro (2016): Seasonality of the Structure and Propagation Characteristics of the MJO. *J. Atmos. Sci.*, **73**, 3511–3526, doi: 10.1175/JAS-D-15-0232.1.

Andersen, J. A., and Z. Kuang (2012): Moist static energy budget of MJO-like disturbances in the atmosphere of a zonally symmetric aquaplanet. *J. Climate*, **25**, 2782–2804, doi:10.1175/JCLI-D-11-00168.1.

Anderson, J. L., et al. (2004), The new GFDL global atmosphere and land model AM2–LM2: Evaluation with prescribed SST simulations, *J. Clim.*, **17**(24), 4641–4673, doi:10.1175/JCLI-3223.1.

Araligidad, N. M., and E. D. Maloney (2008), Wind-driven latent heat flux and the intraseasonal oscillation, Geophys. Res. Lett., 35, L04815, doi:10.1029/2007GL032746.

Arnold, N. P., Z. Kuang, and E. Tziperman (2013): Enhanced MJO-like variability at high SST. *J. Climate*, **26**, 988–1001, doi:10.1175/JCLI-D-12-00272.1.

Arnold, N. P., and D. A. Randall (2015): Global-scale convective aggregation: Implications for the Madden-Julian Oscillation. *J. Adv. Model. Earth Syst.*, **7**, 1499–1518.

Bergman, J. W., H. H. Hendon, and K. M. Weickmann (2001), Intraseasonal air-sea interactions at the onset of El Niño, *J. Clim.*, **14**, 1702–1719, doi: 10.1175/1520-0442(2001)014<1702:IASIAT>2.0.CO;2.

Bessafi, M., and M. C. Wheeler (2006), Modulation of south Indian Ocean tropical cyclones by the Madden-Julian Oscillation and convectively coupled equatorial waves, *Mon. Weather Rev.*, **134**, 638–656, doi: 10.1175/MWR3087.1.

Bretherton, C. S., M. E. Peters, and L. E. Back (2004): Relationships between water vapor path and precipitation over the tropical oceans. *J. Climate*, **17**, 1517–1528, doi:10.1175/1520-0442(2004)017<1517:RBWVPA>2.0.CO;2.

Bony, S. and K.A. Emanuel (2005): On the Role of Moist Processes in Tropical Intraseasonal Variability: Cloud–Radiation and Moisture–Convection Feedbacks. *J. Atmos. Sci.*, 62, 2770–2789, doi: 10.1175/JAS3506.1

Chao, W. C., and B. D.Chen (2001), The role of surface friction in tropical intraseasonal oscillation, *Mon. Weather Rev.*, **129**, 896–904, doi: 10.1175/1520-0493(2001)129<0896:TROSFI>2.0.CO;2.

Chikira, M. and M. Sugiyama (2013): Eastward-Propagating Intraseasonal Oscillation Represented by Chikira–Sugiyama Cumulus Parameterization. Part I: Comparison with Observation and Reanalysis. *J. Atmos. Sci.*, **70**, 3920–3939, doi: 10.1175/JAS-D-13-034.1.

Crueger, T., and B. Stevens (2015): The effect of atmospheric radiative heating by clouds on the Madden-Julian Oscillation. *J. Adv. Model. Earth Syst.*, **7**, 854–864, doi:10.1002/2015MS000434.

Das, S., D. Sengupta, A. Chakraborty, J. Sukhatme, and R. Murtugudde, 2016: Low-frequency intraseasonal variability in a zonally symmetric aquaplanet model. *Meteorol. Atmos. Phys.*, **128**, 697–713.

DeMott, C.A., C. Stan, D.A. Randall, and M.D. Branson (2014): Intraseasonal variability in coupled GCMs: the roles of ocean feedbacks and model physics. *J. Climate*,**27**, 4970–4995, doi: 10.1175/JCLI-D-13-00760.1.

de Szoeke, S.P., J.B. Edson, J.R. Marion, C.W. Fairall, and L. Bariteau, 2015: The MJO and Air–Sea Interaction in TOGA COARE and DYNAMO. *J. Climate*, **28**, 597–622, doi: 10.1175/JCLI-D-14-00477.1.

Emanuel, K. A. (1987), An air-sea interaction-model of intraseasonal oscillations in the tropics, *J. Atmos. Sci.*, **44**, 2324–2340, doi: 10.1175/1520-0469(1987)044<2324:AASIMO>2.0.CO;2.

Emanuel, K. A. (1993), The effect of convective response time on WISHE modes, *J. Atmos. Sci.*, 50, 1763–1775.

Emanuel, K. A., David Neelin, J. and Bretherton, C. S. (1994), On large-scale circulations in convecting atmospheres. *Q. J. R. Meteorol. Soc*., 120: 1111–1143. doi:10.1002/qj.49712051902.

Fuchs, Ž., and D. J. Raymond (2002), Large-scale modes of a nonrotating atmosphere with water vapor and cloud-radiation feedbacks, J. Atmos. Sci., 59, 1669–1679, doi: 10.1175/1520-0469(2002)059<1669:LSMOAN>2.0.CO;2

Fuchs, Ž., and D. J. Raymond (2005), Large-scale modes in a rotating atmosphere with radiative-convective instability and WISHE, J. Atmos. Sci., 62, 4084–4094, doi: 10.1175/JAS3582.1.

Fuchs, Ž. and D. J. Raymond (2017), A simple model of intraseasonal oscillations, J. Adv. Model. Earth Syst., 9, 1195–1211, doi:10.1002/2017MS000963.

Guan, B., D.E. Waliser, N.P. Molotch, E.J. Fetzer, and P.J. Neiman (2012): Does the Madden–Julian Oscillation Influence Wintertime Atmospheric Rivers and Snowpack in the Sierra Nevada?. *Mon. Wea. Rev.*, **140**, 325–342, doi: 10.1175/MWR-D-11-00087.1.

Grabowski, W. W. (2003), MJO-like coherent structures: Sensitivity simulations using the cloud-resolving convection parameterization (CRCP), *J. Atmos. Sci.*, **60**, 847–864, doi: 10.1175/1520-0469(2003)060<0847:MLCSSS>2.0.CO;2.

Gonzalez, A. O., and X. Jiang (2017), Winter mean lower tropospheric moisture over the Maritime Continent as a climate model diagnostic metric for the propagation of the Madden-Julian oscillation, *Geophys. Res. Lett*., 44, 2588–2596, doi:10.1002/2016GL072430.

Harrop, B. E., and D. L. Hartmann (2016), The role of cloud radiative heating within the atmosphere on the high cloud amount and top-of-atmosphere cloud radiative effect, *J. Adv. Model. Earth Syst*., 8, 1391–1410, doi:10.1002/2016MS000670.

Hess, P. G., D. S. Battisti, and P. J. Rasch, 1993: Maintenance of the intertropical convergence zones and the largescale tropical circulation on a water-covered Earth. *J. Atmos. Sci*., 50, 691–713,

Hendon, H.H. and J. Glick (1997): Intraseasonal Air–Sea Interaction in the Tropical Indian and Pacific Oceans. *J. Climate*, **10**, 647–661, doi: 10.1175/1520-0442(1997)010<0647:IASIIT>2.0.CO;2.

Hu, Q., and D. A. Randall (1994), Low-frequency oscillations in radiative-convective systems, *J. Atmos. Sci.*, **51**, 1089–1099, doi: 10.1175/1520-0469(1994)051<1089:LFOIRC>2.0.CO;2.

Hu, Q., and D. A. Randall (1995), Low-frequency oscillations in radiative convective systems. Part II: An idealized model, *J. Atmos. Sci.*, **52**, 478–490, doi: 10.1175/1520-0469(1995)052<0478:LFOIRC>2.0.CO;2.

Hsu, P. and T. Li, 2012: Role of the Boundary Layer Moisture Asymmetry in Causing the Eastward Propagation of the Madden–Julian Oscillation. *J. Climate*, **25**, 4914–4931, doi: 10.1175/JCLI-D-11-00310.1.

Hsu, P., T. Li, and H. Murakami (2014), Moisture asymmetry and MJO eastward propagation in an aquaplanet general circulation model. *J. Climate*, 27, 8747–8760.

Kang, I., F. Liu, M. Ahn, Y. Yang, and B. Wang (2013): The role of SST structure in convectively coupled Kelvin–Rossby waves and its implications for MJO formation. *J. Climate*, 26, 5915–5930.

Kessler, W. S. (2001), EOF representations of the Madden-Julian Oscillation and its connection with ENSO, *J. Clim.*, **14**, 3055–3061, doi: 10.1175/1520-0442(2001)014<3055:EROTMJ>2.0.CO;2.

Kim, Y.-J., F. X. Giraldo, M. Flatau, C.-S. Liou, and M. S. Peng (2008), A sensitivity study of the Kelvin wave and the Madden-Julian Oscillation in aquaplanet simulations by the Naval Research Laboratory Spectral Element Atmospheric Model, *J. Geophys. Res*., 113, D20102.

Kim, D., A. H. Sobel, and I.-S. Kang (2011), A mechanism denial study on the Madden-Julian Oscillation, J. Adv. Model. Earth Syst., **3**, M12007, doi:10.1029/2011MS000081.

Kim, D., J.-S. Kug, and A. H. Sobel (2014): Propagating versus nonpropagating Madden–Julian oscillation events. *J. Climate*, **27**, 111–125, doi:10.1175/JCLI-D-13-00084.1.

Kim, H.-M. (2017), The impact of the mean moisture bias on the key physics of MJO propagation in the ECMWF reforecast, *J. Geophys. Res. Atmos*., 122, 7772–7784, doi:10.1002/2017JD027005.

Leroux, S., and Coauthors, 2016: Inter-model comparison of subseasonal tropical variability in aquaplanet experiments: Effect of a warm pool. *J. Adv. Model. Earth Syst.*, n/a-n/a.

Lau, K. M., and L. Peng (1987), Origin of low-frequency (intraseasonal) oscillations in the tropical atmosphere. Part I: Basic theory, *J. Atmos. Sci.*, **44**, 950–972, doi: 10.1175/1520-0469(1987)044<0950:OOLFOI>2.0.CO;2.

Lee, M. I., I. S. Kang, J. K. Kim, and B. E. Mapes (2001), Influence of cloud-radiation interaction on simulating tropical intraseasonal oscillation with an atmospheric general circulation model, *J. Geophys. Res.*, **106**, 14,219–14,233.

Leroux, S., G. Bellon, R. Roehrig, M. Caian, N. P. Klingaman, J.-P. Lafore, I. Musat, C. Rio, and S. Tyteca (2016), Inter-model comparison of subseasonal tropical variability in aquaplanet experiments: Effect of a warm pool, J. Adv. Model. Earth Syst., 8, 1526–1551, doi: 10.1002/2016MS000683.

Lin, J., G.N. Kiladis, B.E. Mapes, K.M. Weickmann, K.R. Sperber, W. Lin, M.C. Wheeler, S.D. Schubert, A. Del Genio, L.J. Donner, S. Emori, J. Gueremy, F. Hourdin, P.J. Rasch, E. Roeckner, and J.F. Scinocca (2006): Tropical Intraseasonal Variability in 14 IPCC AR4 Climate Models. Part I: Convective Signals. *J. Climate*, **19**, 2665–2690, doi: 10.1175/JCLI3735.1.

Lim, S.Y., C. Marzin, P. Xavier, C. Chang, and B. Timbal, 2017: Impacts of Boreal Winter Monsoon Cold Surges and the Interaction with MJO on Southeast Asia Rainfall. *J. Climate*, 30, 4267–4281, doi: 10.1175/JCLI-D-16-0546.1

Maloney, E. D., and A. H.Sobel (2004), Surface fluxes and ocean coupling in the tropical intraseasonal oscillation, *J. Clim.*, **17**, 4368–4386, doi: 10.1175/JCLI-3212.1.

Maloney, E. D. (2009): The moist static energy budget of a composite tropical intraseasonal oscillation in a climate model. *J. Climate*, **22**, 711–729, doi:10.1175/2008JCLI2542.1.

Madden, R. A., and P. R. Julian (1971), Detection of a 40–50 day oscillation in the zonal wind in the tropical Pacific, *J. Atmos. Sci.*, **28**, 702–708, doi: 10.1175/1520-0469(1971)028<0702:DOADOI>2.0.CO;2.

Madden, R. A., and P. R. Julian (1972), Description of global-scale circulation cells in the tropics with a 40–50 day period, *J. Atmos. Sci.*, **29**, 1109–1123, doi: 10.1175/1520-0469(1972)029<1109:DOGSCC>2.0.CO;2.

Maloney, E. D., and D. L. Hartmann (2000a), Modulation of eastern North Pacific hurricanes by the Madden-Julian Oscillation, *J. Clim.*, **13**, 1451–1460, doi: 10.1175/1520-0442(2000)013<1451:MOENPH>2.0.CO;2.

Maloney, E. D., and D. L. Hartmann (2000b), Modulation of hurricane activity in the Gulf of Mexico by the Madden-Julian Oscillation, *Science*, **287**, 2002–2004, doi: 10.1126/science.287.5460.2002.

Maloney, E. D., A. H. Sobel, and W. M. Hannah (2010), Intraseasonal Variability in an Aquaplanet General Circulation Model, J. Adv. Model. Earth Syst., 2, 5, doi: 10.3894/JAMES.2010.2.5.

Moorthi, S., and M. J. Suarez (1992), Relaxed Arakawa-Schubert: A parameterization of moist convection for general circulation models, *Mon. Weather Rev.*, **120**(6), 978–1002, doi:10.1175/1520-0493(2000)128<1070:ASFCOT>2.0.CO;2.

Möbis B., and B.Stevens (2012), Factors controlling the position of the Intertropical Convergence Zone on an aquaplanet, *J. Adv. Model. Earth Syst.*, 4, M00A04, doi:10.1029/2012MS000199.

Neelin, J. D., I. M. Held, and K. H. Cook (1987), Evaporation-wind feedback and low-frequency variability in the tropical atmosphere, *J. Atmos. Sci.*, **44**, 2341–2348, doi: 10.1175/1520-0469(1987)044<2341:EWFALF>2.0.CO;2.

Neelin, J. D., and J.-Y. Yu (1994), Modes of tropical variability under convective adjustment and the Madden–Julian oscillation. Part I: Analytical theory. *J. Atmos. Sci.*, **51**, 1876–1894, doi:10.1175/1520-0469(1994)051<1876:MOTVUC>2.0.CO;2.

Pritchard, M.S. and D. Yang (2016): Response of the superparameterized Madden–Julian Oscillation to extreme climate and basic-state variation challenges a moisture mode view. *J. Climate*, 29, 4995–5008.

Raymond, D. J. (2001), A new model of the Madden-Julian Oscillation, *J. Atmos. Sci.*, **58**, 2807–2819, doi: 10.1175/1520-0469(2001)058<2807:ANMOTM>2.0.CO;2.

Riley Dellaripa, E. M. and E. D. Maloney (2015). Analysis of MJO wind-flux feedbacks in the Indian Ocean using RAMA buoy observations. *J. Meteorol. Soc. Jpn., Ser. II*, *93*, 1-20.

Rotstayn, L. D. (1997), A physically based scheme for the treatment of stratiform clouds and precipitation in large-scale models. I: Description and evaluation of the microphysical processes, *Q. J. R. Meteorol. Soc.*, **123**(541), 1227–1282, doi:10.1002/qj.49712354106.

Rotstayn, L. D., B. F. Ryan, and J. J. Katzfey (2000), A scheme for calculation of the liquid fraction in mixed-phase stratiform clouds in large-scale models, *Mon. Weather Rev.*, **128**(4), 1070–1088, doi:10.1175/1520-0493(2000)128<1070:ASFCOT>2.0.CO;2.

Salby, M. L., R. R. Garcia, and H. H. Hendon (1994), Planetary-scale circulations in the presence of climatological and wave-induced heating, *J. Atmos. Sci.*, **51**, 2344–2367, doi: 10.1175/1520-0469(1994)051<2344:PSCITP>2.0.CO;2.

Shi, X., and C. S. Bretherton (2014), Large-scale character of an atmosphere in rotating radiative-convective equilibrium, *J. Adv. Model. Earth Syst.*, 6, 616–629, doi: 10.1002/2014MS000342.

Shinoda, T., H. H. Hendon, and J.Glick (1998), Intraseasonal variability of surface fluxes and sea surface temperature in the tropical western Pacific and Indian Oceans, *J. Clim.*, **11**, 1685–1702, doi: 10.1175/1520-0442(1998)011<1685:IVOSFA>2.0.CO;2.

Sobel, A. H., J. Nilsson, and L. M. Polvani (2001), The weak temperature gradient approximation and balanced tropical moisture waves. *J. Atmos. Sci.*, 58, 3650–3665, doi:10.1175/1520-0469(2001)058<3650:TWTGAA>2.0.CO;2.

Sobel, A. H., E. D. Maloney, G. Bellon, and D. M. Frierson (2008), The role of surface heat fluxes in tropical intraseasonal oscillations, *Nat. Geosci.*, **1**, 653–657, doi: 10.1038/ngeo312.

Sobel, A. H., E. D. Maloney, G. Bellon, and D. M. Frierson (2010), Surface fluxes and tropical intraseasonal variability: A reassessment, *J. Adv. Model. Earth Syst.*, **2**, 2, doi: 10.3894/JAMES.2010.2.2.

Sobel, A. H., and E. Maloney (2012), An idealized semi-empirical framework for modeling the Madden–Julian oscillation. *J. Atmos. Sci.*, 69, 1691–1705, doi:10.1175/JAS-D-11-0118.1.

Sobel, A. H., and E. Maloney (2013), Moisture modes and the eastward propagation of the MJO. *J. Atmos. Sci.*, 70, 187–192, doi:10.1175/JAS-D-12-0189.1.

Sobel, A. H., and S. Gildor (2003), A simple time-dependent model of SST hot spots, *J. Clim.*, **16**, 3978–3992, doi: 10.1175/1520-0442(2003)016<3978:ASTMOS>2.0.CO;2.

Sobel, A. H., S. Wang, and D. Kim (2014): Moist static energy budget of the MJO during DYNAMO. *J. Atmos. Sci.*, 71, 4276–4291, doi:10.1175/JAS-D-14-0052.1.

Swinbank, R., T. N. Palmer, and M. K. Davey (1988): Numerical Simulations of the Madden and Julian Oscillation. *J. Atmos. Sci*., 45, 774–788, doi: 10.1175/1520-0469(1988)045<0774:NSOTMA>2.0.CO;2

Tiedtke, M. (1993): Representation of clouds in large-scale models. *Mon. Wea. Rev*., 121, 3040–3061.

Waliser, D. E. (2006), Intraseasonal Variability, in *The Asian Monsoon*, **844**, edited by B. Wang pp. 203–257, Springer, Heidelberg, Germany.

Wang, B. (1988), Dynamics of tropical low-frequency waves: An analysis of the moist Kelvin wave, *J. Atmos. Sci.*, **45**, 2051–2065, doi: 10.1175/1520-0469(1988)045<2051:DOTLFW>2.0.CO;2.

Wang, B. (2005), Theory, in *Intraseasonal Variability in the Atmosphere-Ocean Climate System*, edited by K. M. Lau and D. E. Waliser pp. 307–360, Springer, Heidelberg, Germany.

Wang, B. (2011): Theory. *Intraseasonal Variability in the Atmosphere-Ocean Climate System*, Springer, 307–360.

Wang, B. and G. Chen (2017), *A general theoretical framework for understanding essential dynamics of Madden–Julian oscillation*. Climate Dynamics, 49(7-8), pp.2309-2328.

Wang, B., and H. Rui (1990), Dynamics of the coupled moist Kelvin-Rossby wave on an equatorial beta-plane, *J. Atmos. Sci.*, **47**, 397–413, doi: 10.1175/1520-0469(1990)047<0397:DOTCMK>2.0.CO;2.

Wang, B., and T. Li (1994), Convective interaction with boundary-layer dynamics in the development of the tropical intraseasonal system, *J. Atmos. Sci.*, **51**, 1386–1400.

Wheeler, M. C., and J. L. McBride (2005), Australian-Indonesian monsoon, in Intraseasonal Variability in the Atmosphere-Ocean Climate System, edited by W. K. M. Lau and D. E. Waliser pp. 125–173, Springer, Heidelberg, Germany.

Yano, J.-I., and K. Emanuel (1991), An improved model of the equatorial troposphere and its coupling with stratosphere, *J. Atmos. Sci.*, 48, 377–389.

Zhang, C. (2005), The Madden-Julian Oscillation, *Rev. Geophys.*, **43**, RG2003, doi: 10.1029/2004RG000158.

Zhang, C., 2013: Madden–Julian Oscillation: Bridging Weather and Climate. *Bull. Amer. Meteor. Soc*., 94, 1849–1870, doi: 10.1175/BAMS-D-12-00026.1

Zhao, C., T. Li, and T. Zhou (2013): Precursor signals and processes associated with MJO initiation over the tropical Indian Ocean. *J. Climate*, **26**, 291–307, doi:10.1175/JCLI-D-12-00113.1.

Zhu, H., and H. Hendon (2015): Role of large-scale moisture advection for simulation of the MJO with increased entrainment. *Quart. J. Roy. Meteor. Soc*., 141, 2127–2136, doi:10.1002/qj.2510.